Reconfigurable Silicon Nanowire-Based Schottky Barrier Transistor for Hydrocarbon Gas Detection: A Comprehensive Study

Kapil Pal[1], Chaitanya Gupta[2], Sagar preet bhardwaj[3], Anil Kumar[4], and Sumit Kale[5]

[1]Delhi Technological University, New Delhi, India

Abstract

This paper presents a comprehensive study of a Reconfigurable Silicon Nanowire-based Schottky Barrier Transistor (RSiNw-SBT) for Hydrocarbon Gas Detection. The performance of an RSiNw-SBT gas sensor has been investigated in the presence of hexane, methanol, isopropanol, and dichloromethane gases. The control gate electrode (conducting polymer) of the sensor functioned as an active site for gas detection, where gas molecules interacted to modulate the device's electrical properties. By conducting comprehensive simulations, including analyses of energy band diagrams, surface potentials, electric fields, transfer characteristics, threshold voltages, transconductance, and subthreshold slope, we investigated the behavior of the sensor. The sensitivity is evaluated for both N-MODE and P-MODE configurations. It is determined that the I_{ON} sensitivity for the N-MODE and P-MODE configurations are 77.82% and 77.47%, respectively. This demonstrates the superior performance of the proposed sensor in detecting variations in gas. The heightened sensitivity holds significant potential for improving reliability and precision in gas sensing applications, which has wide-ranging implications for environmental monitoring, industrial safety, and healthcare.

Keywords: Nanowire, Reconfigurable, Sensitivity, Sensor.

Introduction

Gas sensing technology holds a pivotal role across diverse industries, ranging from environmental monitoring to ensuring industrial safety. The imperative development of advanced gas sensors capable of detecting specific hydrocarbon gases with high sensitivity and selectivity is underscored [1]–[4]. Extensive research on gas-sensitive field-effect transistors (FETs) has been conducted, resulting in various types of FET-based sensors, including catalytic-gate FETs, solid electrolyte-based FETs, suspended-gate FETs, and nanomaterial-based FETs [5]–[9]. While these sensors are renowned for their sensitive and selective detection of hydrogen and ammonia, they are also adept at sensing a multitude of other gases and gas mixtures. Numerous FET-based gas sensors, such as gate all around (GAA)-TFET, dopingless Nanowire FET, and Nanorods, have been developed [10]–[13]. However, there exists a research gap concerning the utilization of reconfigurable silicon nanowire Schottky barrier transistors (RSiNw-SBT) for gas sensing applications [14]–[17]. Offering advantages like reconfigurability, enhanced sensitivity and selectivity, and flexible operation, RSiNw-SBT presents itself as a promising technology across various gas sensing applications.

This paper introduces a pioneering study focusing on RSiNw-SBT for Hydrocarbon Gas Detection. The proposed gas sensor comprises two primary components: a control gate crafted from conductive polymer material and a program gate. While the control gate serves as the detection site for various gases, the program gate facilitates polarity switching of the device. Our research delves into the detection of hexane, methanol, isopropanol, and Dichloromethane gases, showcasing the sensor's adaptability and potential applications. The control gate plays a pivotal role in gas molecule detection by interacting with them, thereby altering the electrical characteristics of the sensor. This interaction induces changes in the charge carrier concentration within the semiconductor channel, influencing the current flow between the source and drain terminals. To evaluate the performance of the proposed Reconfigurable Silicon Nanowire-based Schottky Barrier Transistor (RSiNw-SBT) gas sensor, a comprehensive analysis of simulation results was conducted. Parameters such as energy band diagram, surface potential, electric field distribution, transfer characteristics, threshold voltage, transconductance, and subthreshold slope were thoroughly investigated. Additionally, sensitivity parameters such as threshold voltage (V_{TH}) sensitivity and ON-Current (I_{ON}) sensitivity were examined for both N-MODE and P-MODE configurations to comprehend the sensor's response behaviors. To ensure the accuracy and validity of the findings, the simulation results were meticulously calibrated against experimental data, validating the alignment between simulated results and real-world experimental observations. This reaffirms the robustness of the proposed gas sensor for hydrocarbon gas detection.

Device Structure, Calibration, and Simulation Set-up

The schematic of the RSiNw-SBT gas sensor is depicted in Figure 1(a). This proposed gas sensor architecture comprises two crucial components: a control gate made of Conducting Polymer and a program gate. The control gate electrode functions as the active site for

detecting hydrocarbon gases. Meanwhile, the program gate serves to block undesired charge carriers at the drain-channel interface. Silicon nitride serves as an isolator, effectively separating the control gate and program gate. Nickel silicate material is employed for the source and drain contacts, forming Schottky junctions at the source-channel and drain-channel interfaces. When an RSiNw-SBT gas sensor is exposed to a hydrocarbon gas, the sensing mechanism involves the gas analyte interacting with the sensing material within the control gate electrode. This interaction triggers modulations in the sensor's characteristics, like shifts in threshold voltage or modifications in source-drain current. These changes are a result of the gas molecules interacting with the sensing layers of the RSiNw-SBT gas sensor, leading to variations in its response. By detecting and measuring these variations, the sensor can identify the presence of particular gases, showcasing the sensor's ability to detect and quantify gases through the unique interaction between gas molecules and the sensing material within the sensor's control gate electrode. Table I shows the device parameters of the SINw-SBT gas sensor and Table II represents the gases under investigation. The different gases show a shift in the work function of the conducting polymer.

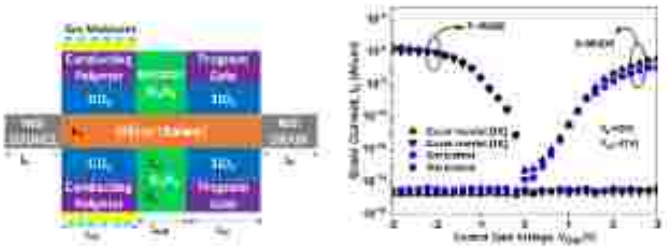

(a) (b)

Fig. 1. Schematic view of (a) RSiNw-SBT gas sensor and (b) Calibration graph.

TABLE I: Device Parameters of the RSiNw-SBT gas sensor

S. No.	Parameters	SB R-Si NW SBT
1.	Source and Drain Metal work-function	4.58 eV
2.	Control Gate Metal work-function	5.18 eV
3.	Program Gate Metal work-function	4.2 eV
4.	Channel Doping Concentration	10^{15} cm^{-3}
5.	Si NW Channel Length	100 nm
6.	Silicon thickness, T_{Si}	10 nm
7.	Gate oxide thickness, T_{OX}	6.5 nm
8.	Gate electrode thickness, T_G	10 nm
9.	Control and Program gate length, L_{CG} and L_{PG}	35 nm and 35 nm
10.	Isolator length, L_{ISO}	30 nm

By plotting the experimental data points against the simulated values, researchers can visually assess the agreement between the two sets of data. In Figure 1(b), a well-calibrated graph shows a close alignment between the experimental and simulated points for both

TABLE II: The reaction of conducting polymer's work function to exposure to different analyte gases was assessed relative to gold (Au).

S. No.	Gases	WF (in N_2) wrt. Au	WF in gas	ΔWF response in gas
1.	Hexane	60 meV	80 meV	20 meV
2.	Methanol	60 meV	100 meV	40 meV
3.	Isopropanol	60 meV	170 meV	110 meV
4.	Dichloromethane	60 meV	210 meV	150 meV

N-MODE and P-MODE configurations. The variation of the control gate voltage ranges from -3V to +3V at a drain-to-source voltage of $\pm 1V$. The simulation results closely match the experimental data, affirming the suitability of the ATLAS TCAD tool for assessing device performance [18].

The performance analysis of the RSiNw-SBT gas sensor is conducted utilizing the Silvaco ATLAS TCAD tool [19]. To capture the tunneling phenomenon at the metal-semiconductor junctions, the Universal Schottky Tunneling model is employed in the simulation [20]–[22]. Furthermore, the simulation incorporates various models such as the Auger model, Fermi Dirac statistics, conmob model, consrh model [23], [24], evt model [25], [26], fnord, boltzman, bqp.qdir=4, temperature=300, and the non-local band-to-band (bbt.nonlocal) tunneling model [27], [28].

Result and Discussion

In this section, we delve into exploring how various hydrocarbon gases impact critical parameters such as the energy band diagram, surface potential, electric field, threshold voltage, subthreshold slope, transconductance, ON-Current, and transfer characteristics. Subsequently, we evaluate the sensitivity of V_{TH} for both N-MODE and P-MODE configurations.

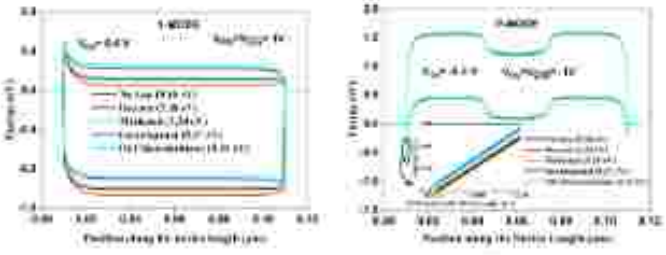

(a) (b)

Fig. 2. Plots of the energy band diagram for different hydrocarbon gases: (a) RSiNw-SBT gas sensor in N-MODE configuration and (b) RSiNw-SBT gas sensor in P-MODE configuration

Figure 2 illustrates the energy band diagram of the RSiNw-SBT gas sensor for both N-MODE and P-MODE configurations. In Fig 2 (a), a work function of 5.16 eV denotes the absence of hydrocarbon gas. The work function of the control gate electrode rises as it interacts with hydrocarbon gas molecules, leading to an

increase in the Schottky barrier width. Consequently, the conduction band shifts upwards, resulting in a reduction in the tunneling rate from the source to the channel. Conversely, in Figure 2 (b), the valence band shifts upwards with an increase in the work function, causing a decrease in the Schottky barrier width and an increase in the tunneling rate of charge carriers.

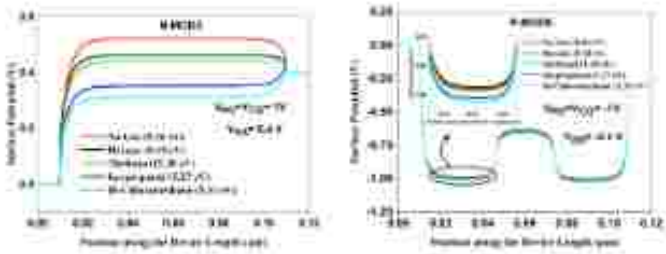

(a) (b)

Fig. 3. Plots of the surface potential for different hydrocarbon gases: (a) RSiNw-SBT gas sensor in N-MODE configuration and (b) RSiNW-SBT gas sensor in P-MODE configuration

Figure 3 displays the surface potential plots of the RSiNw-SBT gas sensor for both N-MODE and P-MODE configurations. In Figure 3 (a), for the N-MODE configuration, the surface potential diminishes with increasing work function of gases. Similarly, in Figure 3 (b), the surface potential under the control-gate electrode decreases with a rise in the work function of gases.

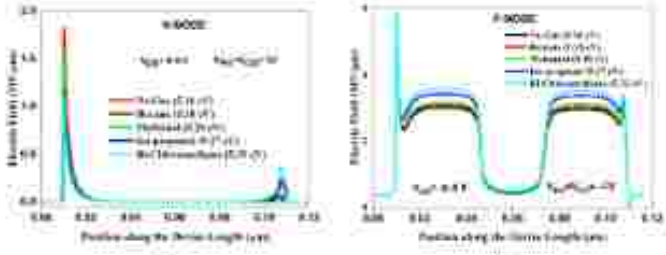

(a) (b)

Fig. 4. Plots of the electric field for different hydrocarbon gases: (a) RSiNw-SBT gas sensor in N-MODE configuration and (b) RSiNw-SBT gas sensor in P-MODE configuration

Figure 4 presents the electric field plot of the RSiNw-SBT gas sensor for both N-MODE and P-MODE configurations. In Figure 4 (a), the electric field decreases as a result of a wider Schottky barrier width and decreased surface potential in the N-MODE configuration. Conversely, in Figure 4 (b), the electric field increases due to the shrinking Schottky barrier width with increasing work function of gases.

Figure 5 showcases the transfer characteristics of the RSiNw-SBT gas sensor for both N-MODE and P-MODE configurations. In Figure 5 (a), the drain current declines with increasing work function of gases, owing to reduced tunneling of charge carriers in the N-MODE configuration. Conversely, in Figure 5 (b), the drain

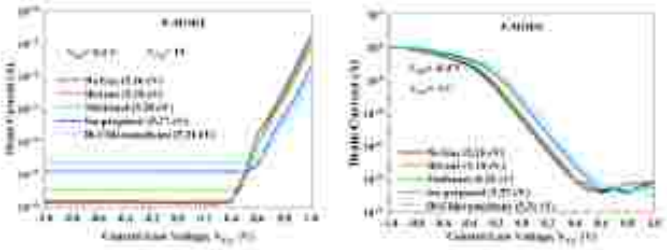

(a) (b)

Fig. 5. Plots of the transfer characteristics for different hydrocarbon gases: (a) RSiNw-SBT gas sensor in N-MODE configuration and (b) RSiNw-SBT gas sensor in P-MODE configuration

current rises due to a decrease in the Schottky barrier width, resulting in an increased tunneling rate.

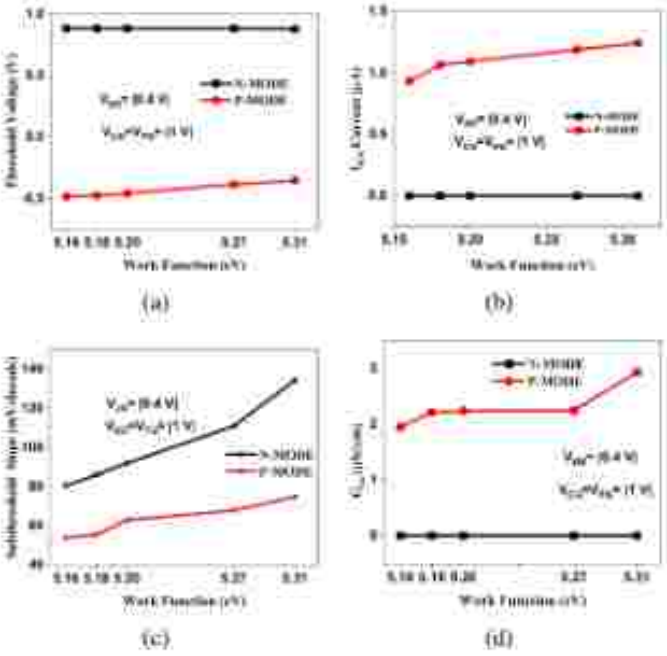

(a) (b) (c) (d)

Fig. 6. The RSiNw-SBT gas sensor (a) Threshold voltage (V_{TH}), (b) I_{ON} Current, (c) Subthreshold Slope (SS), and (d) Transconductance (G_m) for both in N-MODE configuration and P-MODE configuration

Figure 6 depicts plots of threshold voltage, ON-Current, Subthreshold Slope, and transconductance for both N-MODE and P-MODE configurations. In Figure 6 (a), the threshold voltage decreases for N-MODE and increases for P-mode configuration with an increase in the work function of gases. Similarly, in Figure 6 (b), ON-Current increases with the work function of gases for the N-MODE configuration but decreases for the P-MODE configuration. In Figure 6 (c), the subthreshold slope increases with the work function of gases for both N-MODE and P-MODE configurations. Finally, in Figure 6 (d), transconductance decreases with an increase in the work function of gases for the N-MODE configuration, while it increases for the P-MODE configuration.

SENSITIVITY ANALYSIS

In this section, we investigate the performance of the RSiNw-SBT gas sensor in terms of sensitivity. The sensitivity of a gas sensor is a critical performance parameter. To assess the sensitivity of the RSiNw-SBT gas sensor, we analyze the Threshold Voltage (V_{TH}) sensitivity and ON-Current (I_{ON}) sensitivity as outlined below:

$$V_{TH}\ Sensitivity = \frac{V_{TH_{(No\ Gas)}} - V_{TH_{Hydrocarbon}}}{V_{TH_{(No\ Gas)}}} \quad (1)$$

Here, $V_{TH_{(No\ Gas)}} = V_{TH}$ in the absence of Hydrocarbon Gas (WF = 5.16 eV) and $V_{TH_{Hydrocarbon}} = V_{TH}$ in the presence of Hydrocarbon Gas (WF = 5.18 eV, 5.20 eV, 5.27 eV, and 5.31 eV).

Similarly, I_{ON} Sensitivity calculation can be using the below formula:

$$I_{ON}\ Sensitivity = \frac{I_{ON_{(No\ Gas)}} - I_{ON_{Hydrocarbon}}}{I_{ON_{(No\ Gas)}}} \quad (2)$$

Here, $I_{ON_{(No\ Gas)}} = I_{ON}$ in the absence of Hydrocarbon Gas (WF = 5.16 eV) and $I_{ON_{Hydrocarbon}} = I_{ON}$ in the presence of Hydrocarbon Gas (WF = 5.18 eV, 5.20 eV, 5.27 eV, and 5.31 eV).

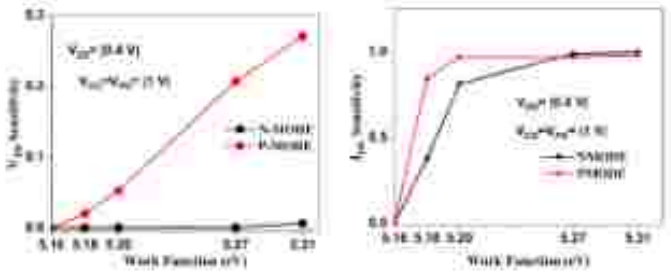

(a) (b)

Fig. 7. Plots of the sensitivity analysis for different hydrocarbon gases: (a) RSiNw-SBT gas sensor in N-MODE configuration and (b) RSiNw-SBT gas sensor in P-MODE configuration

The work function modulation at the Control gate electrode/gate oxide interface of an RSiNw-SBT gas sensor influences the threshold voltage of the device, making it more sensitive to changes in gas concentrations. Illustrated in Figure 7 (a) is the V_{TH} Sensitivity for both N-MODE and P-MODE configurations. It becomes apparent that the V_{TH} Sensitivity escalates with the rise in the work function of the gases. Similarly, depicted in Figure 7 (b) is the I_{ON} Sensitivity, which also increases with the work function of the gases. Both V_{TH} Sensitivity and I_{ON} Sensitivity exhibit a positive correlation with the work function of the gases. The I_{ON} Sensitivity for the proposed gas sensor is higher than the reported gas sensor as depicted in Table III. The I_{ON} sensitivity is 77.82% and 77.47%, respectively, for N-MODE and P-MODE configurations.

TABLE III: Sensitivity comparison of the RSiNw-SBT gas sensor with the state-of-the-art.

S. No.	FET-based Gas Sensors	I_{ON} Sensitivity
1.	SE-JAM-NW FET [29]	0.8
2.	JLNWFET [30]	0.221
3.	GS-JLNWFET [30]	0.245
4.	EG-GS-JLNWFET [30]	0.302
5.	CNWFET [31]	0.315
6.	This work (N-MODE)	0.9906
7.	This work (P-MODE)	0.9808

CONCLUSION

In this work, our investigation into the influence of different hydrocarbon gases on the performance characteristics of an RSiNw-SBT gas sensor has provided valuable insights. By examining parameters such as the energy band diagram, surface potential, electric field, threshold voltage, subthreshold slope, transconductance, ON-Current, and transfer characteristics, we have elucidated the intricate relationship between gas interaction and device behavior. Key findings indicate that modulation of the work function at the control gate electrode/gate oxide interface significantly impacts the sensor's sensitivity to changes in gas concentrations. The I_{ON} sensitivity is 77.82% and 77.47% respectively, for N-MODE and P-MODE configurations, demonstrating the proposed sensor's superior performance in detecting gas variations. This enhanced sensitivity underscores the potential for improved reliability and sensitivity in gas sensing applications, with implications for environmental monitoring, industrial safety, and healthcare.

ACKNOWLEDGMENT

The Science and Engineering Research Board, Department of Science and Technology, Government of India, is funding this work with grant number EEQ/2021/000831.

REFERENCES

[1] N. Yamazoe, "Toward innovations of gas sensor technology," *Sensors and Actuators B: Chemical*, vol. 108, no. 1-2, pp. 2–14, 2005.

[2] N. Yamazoe and K. Shimanoe, "New perspectives of gas sensor technology," *Sensors and Actuators B: Chemical*, vol. 138, no. 1, pp. 100–107, 2009.

[3] S. Mao, J. Chang, H. Pu, G. Lu, Q. He, H. Zhang, and J. Chen, "Two-dimensional nanomaterial-based field-effect transistors for chemical and biological sensing," *Chemical Society Reviews*, vol. 46, no. 22, pp. 6872–6904, 2017.

[4] D. H. Kwak, Y. Seo, J. E. Anthony, S. Kim, J. Hur, H. Chae, H. J. Park, B.-G. Kim, E. Lee, S. Ko *et al.*, "Enhanced gas sensing performance of organic field-effect transistors by modulating the dimensions of triethylsilylethynyl-anthradithiophene microcrystal arrays," *Advanced Materials Interfaces*, vol. 7, no. 4, p. 1901696, 2020.

[5] S. Singh, M. Khosla, G. Wadhwa, and B. Raj, "Design and analysis of double-gate junctionless vertical tfet for gas sensing applications," *Applied Physics A*, vol. 127, pp. 1–7, 2021.

[6] X. Liu, S. Cheng, H. Liu, S. Hu, D. Zhang, and H. Ning, "A survey on gas sensing technology," *Sensors*, vol. 12, no. 7, pp. 9635–9665, 2012.

[7] S. Singh, A. Sharma, V. Kumar, P. Umar, A. K. Rao, and A. K. Singh, "Investigation of n+ sige juntionless vertical tfet with gate stack for gas sensing application," *Applied Physics A*, vol. 127, no. 9, p. 726, 2021.

[8] A. L. Spetz, M. Skoglundh, and L. Ojamäe, "Fet gas-sensing mechanism, experimental and theoretical studies," in *Solid state gas sensing*. Springer, 2008, pp. 1–27.

[9] T.-Y. Chen, H.-I. Chen, C. S. Hsu, C.-C. Huang, C.-F. Chang, P.-C. Chou, and W.-C. Liu, "On an ammonia gas sensor based on a pt/algan heterostructure field-effect transistor," *IEEE electron device letters*, vol. 33, no. 4, pp. 612–614, 2012.

[10] J. Madan and R. Chaujar, "Palladium gate all around-hetero dielectric tunnel fet based highly sensitive hydrogen gas sensor," *Superlattices and Microstructures*, vol. 100, pp. 401–408, 2016.

[11] N. Jayaswal, A. Raman, N. Kumar, and S. Singh, "Design and analysis of electrostatic-charge plasma based dopingless igzo vertical nanowire fet for ammonia gas sensing," *Superlattices and Microstructures*, vol. 125, pp. 256–270, 2019.

[12] P. Feng, F. Shao, Y. Shi, and Q. Wan, "Gas sensors based on semiconducting nanowire field-effect transistors," *Sensors*, vol. 14, no. 9, pp. 17406–17429, 2014.

[13] A. Raman, D. Kakkar, M. Bansal, and N. Kumar, "Design and performance analysis of gaa schottky barrier-gate stack-dopingless nanowire fet for phosphine gas detection," *Applied Physics A*, vol. 125, pp. 1–11, 2019.

[14] M. Arafat, B. Dinan, S. A. Akbar, and A. Haseeb, "Gas sensors based on one dimensional nanostructured metal-oxides: a review," *Sensors*, vol. 12, no. 6, pp. 7207–7258, 2012.

[15] S. Ranwa, M. Kumar, J. Singh, M. Fanetti, and M. Kumar, "Schottky-contacted vertically self-aligned zno nanorods for hydrogen gas nanosensor applications," *Journal of Applied Physics*, vol. 118, no. 3, 2015.

[16] R. Gautam, M. Saxena, R. Gupta, and M. Gupta, "Gate-all-around nanowire mosfet with catalytic metal gate for gas sensing applications," *IEEE transactions on nanotechnology*, vol. 12, no. 6, pp. 939–944, 2013.

[17] N. K. Singh, A. Raman, S. Singh, and N. Kumar, "A novel high mobility in1-xgaxas cylindrical-gate-nanowire fet for gas sensing application with enhanced sensitivity," *Superlattices and Microstructures*, vol. 111, pp. 518–528, 2017.

[18] A. Heinzig, S. Slesazeck, F. Kreupl, T. Mikolajick, and W. M. Weber, "Reconfigurable silicon nanowire transistors," *Nano letters*, vol. 12, no. 1, pp. 119–124, 2012.

[19] "Device simulation software, atlas, silvaco int.,santa clara, ca, usa," 2023.

[20] A. Kumar and S. Kale, "A comparative analysis of cavity positions in charge plasma based tunnel fet for biosensor application," *IETE Journal of Research*, pp. 1–14, 2023.

[21] V. Thakur, A. Kumar, and S. Kale, "Analytical modeling of spacer-engineered reconfigurable silicon nanowire schottky barrier transistor for biosensing applications," *Micro and Nanostructures*, p. 207799, 2024.

[22] A. Kumar and S. Kale, "Spacer-engineered reconfigurable silicon nanowire schottky barrier transistor as a label-free biosensor," *Silicon*, pp. 1–14, 2023.

[23] R. Singh, S. Kaim, R. MedhaShree, A. Kumar, and S. Kale, "Dielectric engineered schottky barrier mosfet for biosensor applications: Proposal and investigation," *Silicon*, vol. 14, no. 8, pp. 4053 – 4062, 2022.

[24] A. Kumar and S. Kale, "Dual-k reconfigurable silicon nanowire schottky barrier transistor for biosensing application," in *Proceedings of the 8th IEEE Electron Devices Technology and Manufacturing (EDTM) Conference*, Bangalore, India, Mar. 3-6 2024.

[25] S. Kale and P. N. Kondekar, "Design and investigation of dielectric engineered dopant segregated schottky barrier mosfet with nisi source/drain," *IEEE Transactions on Electron Devices*, vol. 64, no. 11, pp. 4400–4407, 2017.

[26] S. Kale, N. H. Latha, and L. K. Bramhane, "Design and proposal of double pocket schottky barrier tfet with dielectric modulation for biosensors applications," *Silicon*, vol. 14, no. 16, pp. 10957–10966, 2022.

[27] N. H. Latha and S. Kale, "Dielectric modulated schottky barrier tfet for the application as label-free biosensor," *Silicon*, vol. 12, no. 11, pp. 2673–2679, 2020.

[28] S. Kale, "Investigation of dual metal gate schottky barrier mosfet for suppression of ambipolar current," *IETE Journal of Research*, vol. 69, no. 1, pp. 404–409, 2023.

[29] N. Neeraj, S. Sharma, A. Goel, S. Rewari, S. Deswal, and R. Gupta, "Modeling and simulation characteristics of a highly-sensitive stack-engineered junctionless accumulation nanowire fet for ph3 gas detector," *ECS Journal of Solid State Science and Technology*, 2024.

[30] N. Singh, R. Kar, and D. Mandal, "Simulation and analysis of zno-based extended-gate gate-stack junctionless nwfet for hydrogen gas detection," *Applied Physics A*, vol. 127, no. 4, p. 290, 2021.

[31] C. Verma, J. Singh, S. K. Tripathi, and R. Kumar, "Design and performance analysis of ultrathin nanowire fet ammonia gas sensor," *Silicon*, vol. 14, no. 11, pp. 6321–6327, 2022.